Chapter 2
Strong Laser Fields and Ultrashort Laser Pulses

The creation of strong laser fields is closely related to the formation of short laser pulses giving access to very high intensities while keeping the average power of the laser system on a moderate and thus experimentally feasible level. Usually, in addition to this strong temporal confinement of the energy, the laser beam is also focussed spatially. This chapter gives an overview about ultrashort laser pulses and the strong fields they are associated with. It is organized as follows: First, in Sect. 2.1 the mathematical framework as commonly used for the description of short laser pulses is summarized. It also covers the properties and the description of electromagnetic fields in laser resonators and in particular the concepts underlying *mode-locking* as a key technique in modern ultrashort pulse generation. Here, the focus lies on *Kerr-lens mode-locked Ti:sapphire*[1] laser systems since these represent the standard table-top system used in many laboratories as well as in the experimental setup used in this work. Then, in Sect. 2.2, the specific laser system and subsequent pulse manipulation techniques as used in this work are discussed involving also the treatment of important nonlinear effects in matter.

2.1 Mathematical Description of Laser Pulses

This section gives a short summary about the mathematical description of short laser pulses. It follows the descriptions which can be found in standard laser physics textbooks, e.g. [4, 8, 11, 21, 40]. Particular information about ultrashort laser pulses and the associated phenomena are reviewed e.g. in [5, 10, 18, 22].

If the polarization and transverse properties of a laser beam are neglected, monochromatic light emitted from a laser system can be characterized at any (fixed) point in space by its oscillating electric field $E(t) = \mathrm{Re}\{E \exp[i\omega t]\}$ [9, Sect. 7.3] where E is the field amplitude and ω_L the angular laser frequency. The continuous wave

[1] Titanium-ion doped sapphire ($Ti:Al_2O_3$).

L. Fechner, *High-Resolution Experiments on Strong-Field Ionization of Atoms and Molecules*, Springer Theses, DOI 10.1007/978-3-319-32046-5_2

oscillates with constant amplitude and the laser thus represents the extreme antonym of a suitable system for the generation of ultrashort pulses. In fact, lasers with an emission characteristic close to this hypothetical system, as e.g. the Helium-neon laser (HeNe laser) are commonly referred to as *continuous-wave* (cw) laser systems. To extend the description to non-monochromatic laser sources, an arbitrary spectral amplitude $\tilde{E}(\omega)$ of finite width is introduced and the resulting field may be described as, see e.g. [40, appendix G],

$$E(t) = \mathrm{Re}\left\{\frac{1}{\sqrt{2\pi}}\int_{-\infty}^{\infty} \mathrm{d}\omega \tilde{E}(\omega)\exp[i\omega t]\right\} \tag{2.1}$$

$$= \mathrm{Re}\left\{\frac{1}{\sqrt{2\pi}}\int_{-\infty}^{\infty} \mathrm{d}\omega \tilde{A}(\omega)\exp[i(\omega t + \varphi(\omega))]\right\}, \tag{2.2}$$

where the factor $1/\sqrt{2\pi}$ preceding the integral is arbitrarily chosen. The complex field amplitude $\tilde{E}(\omega) = \tilde{A}(\omega)\exp[i\varphi(\omega)]$ is not accessible in the experiment, however, the spectral intensity $I(\omega) = E^*(\omega)E(\omega)$ may be measured with a spectrometer. In contrast, $\tilde{A}(\omega)$ is real, representing the modulus of a complex number. In particular Eq. (2.2) allows a fairly intuitive interpretation: The total electric field $E(t)$ is formed by a continuous superposition of harmonically oscillating fields with individual contributions to the total field characterized by an amplitude $\tilde{A}(\omega)$. In addition, each of the contributing fields may have an individual phase shift $\varphi(\omega)$. Equation (2.1) can be directly identified with the Fourier transform [6, Sect. 15.3.1.2], relating $E(t)$ in the time domain with $\tilde{E}(\omega)$ in the frequency domain:

$$E(t) = \mathcal{F}\left\{\tilde{E}(\omega)\right\}. \tag{2.3}$$

The inverse transformation is then given by

$$\tilde{E}(\omega) = \mathcal{F}^{-1}\left\{E(t)\right\} = \frac{1}{\sqrt{2\pi}}\int_{-\infty}^{\infty} \mathrm{d}t\, E(t)\exp[-i\omega t]. \tag{2.4}$$

The special case of monochromatic radiation can easily be obtained from Eq. (2.4) with $\tilde{E}(\omega) = \delta(\omega-\omega_\mathrm{L})/\sqrt{2\pi}$. Further details about the mathematical treatment can be found in literature, e.g. in [10, 40], and will not be discussed here in detail.

The Fourier transform, connecting the spectral and the temporal representation of the laser field, causes an intrinsic and fundamental connection between the spectral width[2] $\Delta\omega$ and the minimum pulse duration $\Delta\tau_\mathrm{F}$ achievable. If Gaussian profiles are presumed, $E(t) \propto \exp\left[-4\ln(2)t^2/\Delta\tau_\mathrm{F}^2\right]$ and $\tilde{E}(\omega) \propto \exp\left[-4\ln(2)\omega^2/\Delta\omega^2\right]$, Eq. (2.1) yields

$$\Delta\tau_\mathrm{F}' = \frac{8\ln(2)}{\Delta\omega'}. \tag{2.5}$$

[2] The term "width" is used here and in the following as a synonym for "full width at half maximum" (FWHM).

However, due to the important role of the intensity $I = E^2$ in the interaction with atoms and molecules, see Sect. 3.1, often the temporal and spectral distributions $I(t)$ and $I(\omega)$ are of more interest than the electric fields. If the width of these distributions is denoted with $\Delta\tau_\mathrm{F}$ and $\Delta\omega$, respectively, it follows directly from the properties of the Gaussian distribution $\Delta\tau'_\mathrm{F} = \sqrt{2}\Delta\tau_\mathrm{F}$ and $\Delta\omega' = \sqrt{2}\Delta\omega$ and thus with Eq. (2.5):

$$\Delta\tau_\mathrm{F} = \frac{4\ln(2)}{\Delta\omega}. \tag{2.6}$$

Although discussed here for the special case of Gaussian profiles, similar relations of the form $\Delta\tau_\mathrm{F} = {}^{\mathrm{const}}/_{\Delta\omega}$ can be established for other distributions, see e.g. [40, Sect. 8.6.1]. It can be concluded that the duration of the pulses is generally limited by the spectral width of the laser system. It should be noted that $\tilde{E}(\omega)$ was chosen as a real value, thus $\varphi(\omega) \equiv 0$. As will be shown in the following section, any other choice of the phase will either not influence or lengthen the pulse duration. In the example above, however, the pulse duration is limited *only* by the bandwidth of the laser and the mathematical property of the Fourier transform, therefore such ideal laser pulses are commonly called *Fourier-limited pulses*. The discussion of the monochromatic laser at the beginning of this section can now be put in simple equations: From $\Delta\omega = 0$ follows with Eq. (2.6) $\Delta\tau_\mathrm{F} = \infty$.

2.1.1 Laser Pulses as Superpositions of Resonator Modes

For the generation of short laser pulses, the additional constraints arise due to the resonator introducing boundary conditions for the electric field. In a resonator of optical length d with infinitely large planar end-mirrors the condition is simply given by ${}^{\omega}/_{2\pi} = {}^{qc}/_{2d}$ where $q > 0$ is an integer number and c the speed of light in vacuum [8, Sect. 2.1]. The stationary field configurations in the resonator, commonly known as *resonator eigenmodes* or simply *resonator modes*, are given by standing plane waves fulfilling the condition for an arbitrary choice of q. In addition, the resonator modes are fully characterized by this number. However, for resonators with finite mirror diameters, the situation is substantially different. Caused by continuous diffraction losses which depend on the distance to the resonator axis, planar waves are no longer eigenmodes, see e.g. [8, Sect. 5.2.2].

For symmetric *confocal resonators* with spherical mirrors, where d is twice the focal length of the mirrors, new solutions have been found analytically, first for the special case of identical square resonator mirrors [2], later for more general configurations including circular shaped mirrors [3]. These solutions are commonly referred to as *transverse electromagnetic modes* (TEM modes), characterized by three integer numbers $q, m, n > 0$ and denoted as $\mathrm{TEM}_{m,n,q}$, see e.g. [8, Sect. 5.2.3]. The transverse field amplitude in the modes is characterized by m and n and is of Gaussian shape for all $\mathrm{TEM}_{0,0,q}$ modes which are usually called *fundamental modes*.

The frequency depends on all three numbers and is, in the case of identical circular resonator mirrors in confocal configuration, given by [2, 3]

$$\frac{\omega}{2\pi} = \frac{c}{2d} \cdot \begin{cases} q + \frac{1}{2}(2m + n + 1) & \text{circular mirrors} \\ q + \frac{1}{2}(m + n + 1) & \text{square mirrors.} \end{cases} \tag{2.7}$$

Obviously, in both cases, different $\mathrm{TEM}_{m,n,q}$ modes comprise the same frequency and thus are energetically degenerated. Compared to the hypothetical case of infinitely large mirrors mentioned before, new frequencies are accessible for appropriate combinations of m and n with $2m + n + 1$ and $m + n + 1$ being odd for circular and square mirrors, respectively. These frequencies are centered right in the middle between those of the fundamental modes. Thus, the frequency difference between two adjacent modes of the resonator, the *free spectral range* (FSR) is given by [8, Sect. 5.2.8]

$$\frac{\delta\omega_{\mathrm{FSR}}}{2\pi} = \frac{c}{4d}. \tag{2.8}$$

Since non-fundamental modes exhibit intensity profiles less confined on the resonator axis, an appropriate aperture or choice of the ratio between the mirror diameters and d can be used to increase their relative diffraction losses and thus to force the laser into the fundamental modes, see e.g. [21, Sect. 8.1.]. For convenience, the absence of non-fundamental modes is assumed in the following, $m = n \equiv 0$. The frequency difference between two adjacent *fundamental* modes oscillating in the resonator is given by [8, Sect. 5.2.8]

$$\frac{\delta\omega}{2\pi} = 2\frac{\delta\omega_{\mathrm{FSR}}}{2\pi} = \frac{c}{2d}. \tag{2.9}$$

Provided, the amplification by the active laser medium is sufficiently high, all resonator modes in a certain spectral range may contribute to the formation of the overall electric field emitted by the system. If the emission spectrum of the active medium is assumed to be of Gaussian shape centered around ω_0 with a width $\Delta\omega$ fulfilling $\delta\omega \ll \Delta\omega \ll \omega_0$ and the phase relation between adjacent modes is further assumed to be constant, $\delta\varphi = \mathrm{const}$, the total field Eq. (2.2) can be written as [40, Sect. 8.6.1.]

$$\begin{aligned} E(t) &= \mathrm{Re}\left\{ \frac{1}{\sqrt{2\pi}} \sum_{l=-\infty}^{\infty} \tilde{A}(\omega_0 + l\delta\omega) \exp\left[i((\omega_0 + l\delta\omega)t + l\delta\varphi)\right] \right\} \\ &= \mathrm{Re}\left\{ \frac{1}{\sqrt{2\pi}} \left(\sum_{l=-\infty}^{\infty} \tilde{A}(\omega_0 + l\delta\omega) \exp\left[il\delta\varphi\right] \exp\left[il\delta\omega t\right] \right) \exp\left[i\omega_0 t\right] \right\} \\ &= \mathrm{Re}\left\{ \frac{1}{\sqrt{2\pi}} A(t) \exp\left[i\omega_0 t\right] \right\}. \end{aligned} \tag{2.10}$$

In the last step, the expression in brackets was identified as a discrete version of the Fourier transform and the existence of an appropriate function $A(t)$ was deduced.

As derived e.g. in [40, Sect. 8.6.1.], the electric field is oscillating with a *carrier frequency* ω_0 and is modulated in amplitude by a time-dependent function $A(t)$ commonly referred to as *pulse envelope*. Further, for the separation of the pulses in time τ and their duration $\Delta\tau$ it can be derived [40, Sect. 8.6.1.]

$$\tau = {}^{2\pi}/_{\delta\omega} \tag{2.11}$$

$$\Delta\tau = {}^{4\ln(2)}/_{\Delta\omega}. \tag{2.12}$$

From Eqs. (2.11) and (2.9) follows $\tau = {}^{2d}/_{c}$ meaning that the repetition rate of the laser system is simply determined by the round-trip time of the laser pulses in the resonator [40, Sect. 8.6.2]. Equation (2.12) is identical to the previously found general expression, Eq. (2.6). From this it can be concluded that the superposition of resonator modes with constant phase differences of adjacent modes produces Fourier limited pulses. This situation is commonly referred to as *mode-locked* operation of the laser. In suitable materials, as e.g. Ti:sapphire crystals, $\Delta\omega$ can be large enough to cause simultaneously significant amplification for a certain wavelength λ_1 and even its second harmonic $\lambda_2 = 2\lambda_1$ [12] which is commonly called an *octave-spanning* spectrum. In this situation, $\Delta\tau_F$ can become very short, even of the same order of the oscillation period of the electromagnetic wave itself. Such pulses are commonly referred to as *few-cycle pulses* [5]. It is noteworthy that the peak intensity in such laser pulses is proportional to the square of the number of modes contributing, see e.g. [40, Sect. 8.6.1.].

The most general form for the phase $\varphi(\omega)$ guaranteeing the generation of Fourier limited pulses is given by

$$\varphi(\omega) = \varphi(\omega_0) + a \cdot (\omega - \omega_0)\,, \tag{2.13}$$

where a is a constant and the function $\varphi\,(\omega)$ is only evaluated for the discrete resonator frequencies. This equation may be interpreted as a Taylor series [6, Sect. 6.1.4.5] of an arbitrary function $\varphi(\omega)$ around ω_0 up to the first order. It is self-evident and often also convenient to extend this to

$$\varphi(\omega) = \varphi(\omega_0) + \left.\frac{\partial\varphi(\omega)}{\partial\omega}\right|_{\omega=\omega_0} (\omega - \omega_0) + \frac{1}{2}\left.\frac{\partial^2\varphi(\omega)}{\partial\omega^2}\right|_{\omega=\omega_0} (\omega - \omega_0)^2 + \mathcal{O}\left(\omega^3\right), \tag{2.14}$$

see e.g. [35, Sect. 9.1]. The influence of the different terms on the shape of the generated pulses are displayed in Fig. 2.1 calculated for a model resonator and active medium. Although the number of modes contributing is much less than in a typical laser setup for ultrashort laser pulses, general qualitative features can be studied. The figure depicts eight spectral field distributions $\tilde{A}(\omega)$ of Gaussian shape evaluated at the positions of the resonator modes (blue line and dots in left pictures). The spectral phase $\varphi(\omega)$ is shown in green. $E(t)$ is then calculated with Eq. (2.10), where the summation can be restricted to a finite number of modes with significant amplitudes

without noticeable change of the result. $E(t)$ is shown on the right as a blue line, while the red line shows the envelope function calculated by replacing Re{} by Abs{} in Eq. (2.10).

In Fig. 2.1a, the width of the emission spectrum is fairly narrow such that only three modes significantly contribute to the total electric field, resulting in a beat frequency. The phase in this example is globally set to zero, $\varphi(\omega) \equiv 0$. If the spectrum is chosen broader and broader along (b) and (c), well separated pulses arise which become shorter and shorter. The electric field shown in (c) represents a few-cycle Fourier limited pulse. If a constant global phase is added as done in (d), where $\varphi(\omega) = -\pi$, the envelope and thus the pulse duration is not affected. However, the phase offset between the carrier wave and the envelope, commonly referred to as *carrier-envelope phase* (CEP), see e.g. [5, 29, 32], is altered. Since CEP effects are not explicitly studied in this work and their presence only used as an indicator for the pulse duration, see Sect. 2.2.2, the influence of the constant phase on the electric field is ignored in the following.

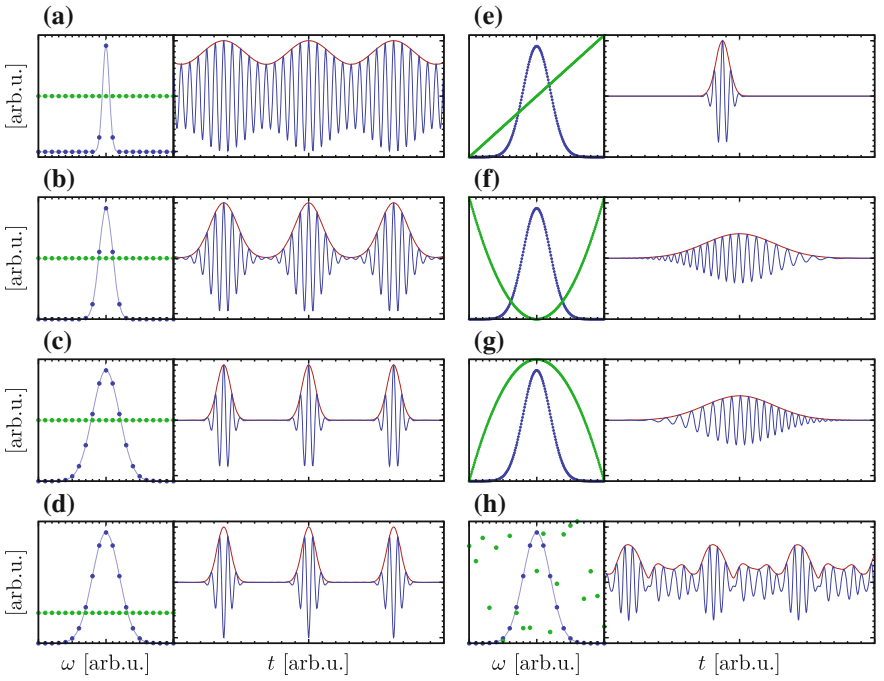

Fig. 2.1 Examples for electric fields created by superpositions of resonator modes. Each figure contains of two plots: In the *left*, the spectral amplitude $\tilde{A}(\omega)$ and the spectral phase $\varphi(\omega)$ are shown in *blue* and *green*, respectively. The functions are evaluated at the discrete frequencies of the resonator modes. In the *right* picture, the resulting electric field is shown in *blue*, the envelope function in *red*, see text for details

As discussed earlier, even a linear trend in $\varphi(\omega)$ guarantees the generation of Fourier limited pulses, see Eq. (2.13). This situation is depicted in Fig. 2.1e, where the pulses from (c) are exactly reproduced despite being shifted on the absolute timescale. Apart from this, the spacing between the modes was decreased, modeling a lengthening of the resonator, see Eq. (2.9). Consequently the round-trip time increases such that the preceding and the following pulses are not visible in the picture any further. For a quadratic trend in $\varphi(\omega)$, however, the situation changes substantially. Even though the spectral amplitudes are identical to the previous case, this phase relation leads to much longer pulses as depicted in Fig. 2.1f, g. In addition, the frequency of the carrier wave changes along the pulse which is commonly known as *chirp*, see e.g. [35, Sect. 9.1]. Finally the case of a random phase relation is shown in (h). The electric field produced seems to be chaotic, nevertheless it is still periodic and each of the occurring peak-like structures has a duration comparable to the well separated, Fourier limited pulses in (c), see e.g. [40, Sect. 8.6]. In order to make the effects more visible, the frequency spacing of the modes is chosen larger again, as in (a)–(d).

In conclusion, the generation of ultrashort laser pulses requires not only the contribution of many modes with different frequencies but also a fixed phase relation between the different modes as close as possible to Eq. (2.13), the ideal mode-locking condition. In reality, the situation becomes more difficult since optical elements in the beam path and even the air traversed on the way to the actual experiment will certainly change the phase relations due to dispersion, see Sect. 2.1.2.

Kerr Lens Mode-Locking

Different techniques have been developed to obtain mode-locked laser operation for the generation of ultrashort pulses. For an historical review see e.g. [18]. One example mentioned there is the *Kerr lens mode-locking* (KLM), an approach based on the nonlinear optical Kerr-effect in suitable transparent materials. It is widely exploited in Ti:sapphire laser systems and will be discussed in the following.

Although mode-locking is defined and described in the frequency domain, namely with the condition from Eq. (2.13) for adjacent resonator modes, it is feasible and convenient to switch to the time-domain picture: As shown in the previous section, perfect mode-locking occurs if, and only if, the associated laser pulses are Fourier limited. Therefore, if a process inside the resonator is capable of shortening the pulses such that their duration approaches the Fourier limit, the phase relation between the modes will adapt and converge to the associated phase relation.

The basic idea for efficient mode-locking is therefore to artificially lower the quality of the resonator and thus increase the losses for any continuous components of the wave, currently present in the resonator [40, Sect. 8.6.3.2 and Appendix F.2]. Any spiked structure generated in the initially random spontaneous emission of the active medium will gain energy quickly and—after some round-trips in the resonator—may form a short stable pulse. The largely differing peak intensity in the pulsed field configuration can be utilized in this respect in different *passive mode-locking* techniques. For example, a suitable absorbing material, a *fast saturable absorber*, may be inserted into the resonator, absorbing the laser radiation but being saturated and thus

transparent for high intensities [40, Sect. 8.6.3.2 and Appendix F.2]. The saturable absorbance may also be included in the resonator end-mirrors using *semiconductor saturable absorber mirrors* (SESAM) [20].

KLM is likewise a passive mode-locking technique but relies on the non-linear optical Kerr-effect, see e.g. [40, Sect. 8.6.3.2] and thus on refraction rather than absorption. For low field intensities the definition of the refractive index $n_0 = {}^{c}/_{v_{\mathrm{ph}}(\lambda)}$ as a function of the phase velocity of the light $v_{\mathrm{ph}}(\lambda)$ and therefore the wavelength λ is a very good approximation. In contrast, in very strong fields, the refractive index shows an additional dependence on the laser intensity $I(t)$ and is given by [40, Sect. 8.6.3.2]

$$n(t) = n_0 + n_2 I(t). \tag{2.15}$$

The *second order index of refraction* n_2 in this expression is a (very small) positive constant. Typical values are around $10^{-13}\mathrm{cm}^2/\mathrm{W}$ to $10^{-17}\mathrm{cm}^2/\mathrm{W}$, see e.g. [4, table 4.1.2], such that the second order term is negligible for low intensities.

With increasing intensity, however, the influence of the second terms grows and for ultrashort strong field can become significant. If a $\mathrm{TEM}_{0,0,q}$ pulse with a Gaussian transverse intensity distribution travels through a non-linear medium inside the resonator, Eq. (2.15) causes a refractive index that changes over the transverse coordinate. Effectively, for $n_2 > 0$ a spherical lens is formed, focusing the beam towards the resonator axis [40, Sect. 8.6.3.2]. This is commonly referred to as *self-focusing*. An aperture or an appropriate geometry of the resonator itself can be used in order to suppress any continuous field components.

If an aperture is present or the geometry of the resonator itself is appropriately chosen, the focusing is required for a sufficient reduction of losses and therefore pulsed field components are favored in the resonator. In each round trip of the pulse, the leading and trailing edge are suppressed due to their lower intensity and the pulse gets shortened [21, Sect. 10.2.2]. One advantage of KLM is the almost instantaneous response of the medium [40, Sect. 8.6.3.2]. Moreover, in particular for Ti:sapphire laser systems, it is beneficial that the laser crystal itself may serve as a non-linear medium for the optical Kerr-effect [19].

2.1.2 Dispersion in Matter

In particular for short laser pulses, dispersion in matter is an important issue due to their large bandwidth according to Eq. (2.12). While traveling along $\hat{e}_z$ through a transparent material, a short laser pulse accumulates a spectral phase of [35, Sect. 7.2]

$$\Phi(\omega) = \frac{n(\omega)\,\omega}{c} z, \tag{2.16}$$

where $n(\omega)$ is the refractive index of the material and c the speed of light in vacuum. Since the carrier frequency ω_0 even of few-cycle pulses is large compared to their

Table 2.1 Definition of phase velocity, group velocity and group velocity dispersion and the relation of this values to (Eq. 2.17) as found e.g. in [35, Sect. 9.1]

Quantity		Relation
Phase velocity	v_{ph}	ω_0/A
Group velocity	v_{g}	$1/B$
Group velocity dispersion	GVD	C

spectral width $\delta\omega$ and the refractive index usually sufficiently smooth, this expression can be approximated by a Taylor expansion, cf. [35, Sect. 9.1]

$$\Phi(\omega) = \underbrace{\Phi(\omega_0)}_{A} + \underbrace{\left.\frac{\partial\Phi(\omega)}{\partial\omega}\right|_{\omega=\omega_0}}_{B}(\omega-\omega_0) + \frac{1}{2}\underbrace{\left.\frac{\partial^2\Phi(\omega)}{\partial\omega^2}\right|_{\omega=\omega_0}}_{C}(\omega-\omega_0)^2 + \mathcal{O}\left(\omega^3\right). \tag{2.17}$$

The three factors A, B and C depend on the characteristics of $n(\omega)$ and are—for fixed ω_0—material constants. Usually, the related quantities listed in Table 2.1 are used for characterization.

The influence of such phase functions on the pulses and their duration was already depicted in Sect. 2.1.1. In particular in the design of femtosecond laser systems also higher orders as the *third order dispersion* (TOD) have to be considered and compensated as accurately as possible, see e.g. [5]. Furthermore, if the phase function is not sufficiently smooth on the scale given by $\Delta\omega$, a (low-order) Taylor expansion might be a less good approximation. Instead, $\Phi(\omega)$ can be derived from $n(\omega)$ which is often well characterized. The pulse shape and duration can then numerically be calculated according to Eq. (2.2). After all, dispersion in media may lead to temporal broadening of short pulses and therefore has to be compensated (or precompensated) in order to obtain short pulses in the experiment.

2.1.3 General Properties of Focussed Laser Beams

Laser beams can be focussed onto a well defined spot using lenses or curved mirrors. Not only the maximum intensity achievable but also a detailed knowledge about the intensity distribution near the focus, the "shape" of the focal volume, is desirable for two reasons: First, the interaction processes between light and matter strongly depends on the intensity, see e.g. Sect. 3.1. Thus, in the case of a gas jet of finite diameter where the laser is focussed on (see Chap. 4), not all atoms will experience the same laser intensity. In fact, an intrinsic averaging over different intensities is present which has to be considered in the interpretation of the data, see e.g. [30]. Second, the geometry of the laser focus is important for the experiment since it defines the interaction region as the spatial overlap with the usually much more extended gas jet, see Sects. 4.1.2 and 4.3.

The intensity of a laser beam can, if exclusively fundamental modes are considered, be described by a Gaussian transverse profile as seen in Sect. 2.1.1. In case of a focussed beam this still holds at any position z_0 along the laser propagation direction $\hat{e}_z$. However the beam diameter then depends on z_0. A focussed beam can therefore be described with [11, Sects. 12.2 and 12.3]

$$I_{z_0}(r) = I_{z_0}^{\max} \cdot \exp\left[-\frac{2r^2}{w^2(z_0)}\right] \tag{2.18}$$

with

$$w(z) = w_0\sqrt{1 + {}^{z^2}/_{z_R^2}}, \tag{2.19}$$

$$w_0 = {}^{\lambda f}/_{\pi R_L}, \tag{2.20}$$

$$z_R = {}^{w_0^2\pi}/_{\lambda}. \tag{2.21}$$

Here, r is the transverse spatial coordinate perpendicular to $\hat{e}_z$, λ the wavelength in the beam, f the focal length of the lens or mirror, R_L the radius of the laser before focusing and z_R the *Rayleigh length*, the distance along $\hat{e}_z$ between the waist of the focus and the point, where its diameter has increased by a factor of $\sqrt{2}$. At this position the intensity has decreased to ${}^1/_2$ of the peak intensity as present in the center of the focus. In contrast to this, $w_0 = w(z = 0)$ describes the transverse distance from the center of the focus to the radius, where the intensity has decreased to ${}^1/_{e^2} \approx {}^1/_{7.4}$. Although both parameters describe the dimensions of the laser focus it is important to keep in mind that they can not simply be related to each other.

$I_{z_0}^{\max}$ denotes the intensity on the beam axis in the plane defined by $z = z_0$. An integration of Eq. (2.18) over φ and r in each of this planes has to yield the same value since the total power of the radiation is preserved. Therefore it is $I_{z_0}^{\max} = ({}^{w_0}/_{w(z_0)})^2\, I^{\max}$ where $I^{\max} = I_{z_0=0}^{\max}$ is the global maximum of the laser intensity. The intensity distribution in the laser focus is thus given by [31, Sect. 2.2]

$$I(z, r) = I^{\max}\left(\frac{w_0}{w(z)}\right)^2 \exp\left[-\frac{2r^2}{w^2(z)}\right]. \tag{2.22}$$

This expression is plotted in Fig. 2.2 for typical parameters of the experiment, namely $\lambda = 790\,\text{nm}$, $f = 7\,\text{cm}$, $R_L = 0.5\,\text{cm}$. Solid red lines represent $w(z)$. The intensity distribution is much more elongated in the propagation direction of the laser than perpendicular to it. Note that the distance shown along z in Fig. 2.2 is 20 times larger than the one shown along r. To emphasize this characteristic feature of laser foci, curves of equal intensity can be calculated. Demanding $I(z, r) = \alpha I^{\max}$ with $\alpha \in [0, 1]$ in Eq. (2.22) yields [31, Sect. 2.2][3]

[3] The original equation contains a typing error which is corrected here.

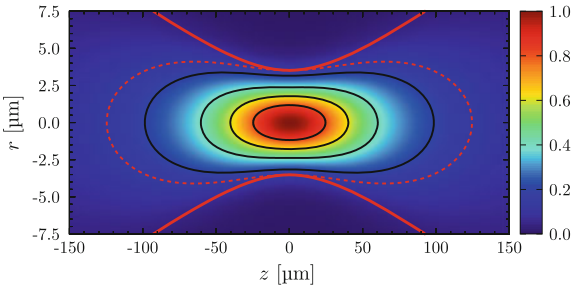

Fig. 2.2 Intensity distribution in a Gaussian laser focus according to Eq. (2.22) with lines of equal intensity (*black solid lines*) calculated with Eq. (2.23) for (from origin) $\alpha = 0.8, 0.6, 0.4, 0.2$, respectively. The positions where the intensity has dropped to $1/e^2$ is shown as *red dashed line*. The parameters used in the calculations are $\lambda = 790\,\text{nm}$, $f = 7\,\text{cm}$, $R_L = 0.5\,\text{cm}$. The *red solid lines* denote $w(z)$ calculated with Eq. (2.19). A similar calculation and illustration of the *contour lines* can be found in [31, Sect. 2.2]

$$r^{\alpha}(z) = \pm\,\text{Re}\left\{\sqrt{\frac{1}{2}w^2(z)\ln\left[\frac{1}{\alpha}\left(\frac{w_0}{w(z)}\right)^2\right]}\right\}. \tag{2.23}$$

The contour lines defined by this relation are shown in Fig. 2.2—starting from the origin outwards—for $\alpha = 0.8, 0.6, 0.4, 0.2$, respectively. The typical extent of the focus with respect to z and r can be calculated with $\alpha_0 = 1/e^2$, shown as dashed red line. The condition $r^{\alpha_0}(z) = 0$ and the calculation of $r^{\alpha_0}(0)$ thus yields

$$\begin{aligned}\Delta r &= 2w_0 \approx 7.0\,\mu\text{m},\\ \Delta z &= 2z_R\sqrt{\left(e^2-1\right)} \approx 250\,\mu\text{m}.\end{aligned} \tag{2.24}$$

Note that Δr also denotes the *diameter* of the laser focus in radial direction rather than the radius. After all, the circumference of the focus along the direction of propagation is much larger than its transverse diameter. As can be seen from Eq. (2.20) and Eq. (2.21), both quantities are proportional to λ. Therefore, light with shorter wavelengths can be focussed "harder", in the case of $\lambda = 395\,\text{nm}$ for example, onto a spot of half the extension in each direction. The relations in this section are only valid for laser beams with perfect Gaussian beam profile. However, real laser beams often show deviations from this ideal situation which is usually described by a value $M^2 \geq 1$ ($= 1$ for a Gaussian profile), see e.g. [11, Sect. 12.5]. As a consequence, the focus dimensions are usually larger than described by Eq. (2.24). Since the aim of this section is more the qualitative description than the derivation of exact numbers, this more complex situation is not treated here.

2.2 Laser Pulse Generation and Manipulation

For the different experiments presented in this thesis, laser pulses of different duration and central wavelength are required. However, in each case, the first step is the generation of strong ultrashort pulses with a commercial femtosecond laser system. These pulses are then modified in different subsequent processes in order to achieve e.g. shorter pulse durations or a different central wavelength.

2.2.1 The Femtosecond Laser System

In all experiments presented in this thesis a commercial *FEMTOLASERS* "FEMTOPOWER compact PRO HP/HR" Ti:sapphire[4] laser system is used as a source for strong and ultrashort laser pulses. General information about Ti:sapphire laser systems can be found e.g. in [10, Sect. 6.7.2] and [40, Sect. 9.2.8]. The specific information about the system used in the experiments are compiled from [14, 15]. The system consists of a mirror-dispersion controlled Ti:sapphire oscillator [37] producing ultrashort ($\lesssim$10 fs), close to Fourier limited, but weak pulses at a high repetition rate. These pulses are stretched in time and subsequently amplified in a second Ti:sapphire crystal in a *chirped pulse amplification* (CPA) scheme [39]. With this technique, damage of the Ti:sapphire crystal in the amplification stage is prevented as it would occur otherwise due to the extreme intensities and thereby caused non-linear effects.

In a multi-pass setup, the laser beam is guided through the amplifier crystal. After the fourth pass, the repetition rate is reduced to around 3 kHz by a Pockels cell. Thus, most of the pulses are suppressed and only one pulse is further amplified in every shot of the pump laser. A description of a very similar amplifier system can be found in [25]. The strong but temporally stretched pulses are compressed in a subsequent prism compressor where a complex interplay of optical prisms and chirped mirrors provide a negative refraction index and at the same time correct for higher order dispersion [36]. The pulse duration is specified to less than 30 fs, the pulse energy to larger than 800 mJ. *Gain narrowing*, the reduction of the spectral width in the amplification process, see e.g. [10, Sect. 7.2.2], mainly causes the increase of the pulse duration compared with the output of the oscillator. In Fig. 2.4a and b, the two spectra can be compared. The overall dispersion of the laser pulses is controlled by third-order dispersion (TOD) precompensation after the oscillator and careful adjustment of the compressor stage. Thus, close to Fourier limited pulses are emitted by the laser system.

[4] Titanium-doped sapphire (Ti:Al_2O_3).

2.2.2 Generation of Few-Cycle Pulses

In the pulses emitted by the laser system, the electric field fulfills more than ten oscillations with a periodicity of approximately 2.6 fs. Even shorter, *few-cycle pulses*, where the pulse duration is in the same order of the field periodicity, see e.g. [5], can be generated in a subsequent process [33]: Since the minimum pulse duration of the pulses delivered by the laser system is limited mainly by the width of the spectral profile, the first step towards shorter pulses is the generation of additional wavelength components. For this, a nonlinear optical effect namely *self-phase modulation* (SPM), see e.g. [4, Sect. 7.5], in a gaseous medium is utilized. Afterwards the pulses can be compressed with specifically designed *chirped mirrors*.

Spectral Broadening by Self-Phase Modulation

In Sect. 2.1, the optical Kerr effect was discussed causing an intensity-dependent refractive index, Eq. (2.15):

$$n(t) = n_0 + n_2 I(t)\,.$$

If the dispersion experienced by an initially Fourier limited $\mathrm{TEM}_{0,0,q}$ pulse, while traveling through a medium of length L with $n_2 > 0 \in \Re$, is neglected, the accumulation of a phase is the only remaining effect [4, Sect. 7.5]:

$$\Phi(t) = -n_2 \frac{\omega_0 L}{c_0} I(t) \tag{2.25}$$

This time-dependent phase shifts the frequencies in the pulse resulting in [4, Sect. 7.5]

$$\begin{aligned} \omega(t) &= \omega_0 + \frac{\mathrm{d}\Phi(t)}{\mathrm{d}t} \\ &= \omega_0 \left(1 - n_2 \frac{L}{c_0} \frac{\mathrm{d}I(t)}{\mathrm{d}t}\right), \end{aligned} \tag{2.26}$$

where $\omega(t)$ is referred to as the *instantaneous frequency* in the pulse. In the leading edge of the pulse, where ${}^{\mathrm{d}I(t)}/_{\mathrm{d}t} > 0$, the frequency is shifted towards lower values while higher frequencies are generated in the trailing edge. Thus, the spectrum of the pulse is broadened and the pulse itself is positively chirped although the temporal pulse shape is not changed in the first instance [10, Sect. 8.1.1]. However, it is of course affected by the usual dispersion in the material. In reality, the situation is much more complex due to effects as self-steepening [4, Sect. 13.3] or finite nonlinear response times [4, table 4.1.1] neglected here. A consequence is e.g. the nonsymmetric broadening of the spectrum visible in Fig. 2.4 not covered by Eq. (2.26) for Fourier limited pulses with symmetric envelope. The enhanced spectral width of the laser light forms the basis of the generation of even shorter pulses.

In the experimental setup schematically shown in Fig. 2.3, the pulses delivered by the laser system are focussed onto a hollow-core glass fiber with an inner diameter of 250 µm. By using a lens with a large focal length of about 1.5 m, the laser

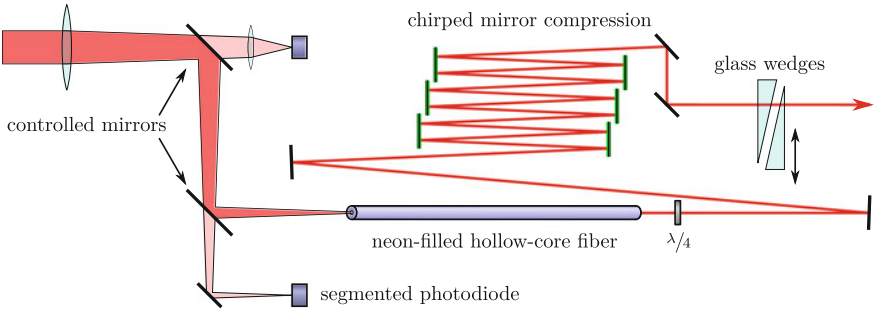

Fig. 2.3 Schematic overview about the setup used for the generation of few-cycle laser pulses. The pulses delivered by the femtosecond laser system are focussed onto a neon-filled hollow-core fiber filled with neon. The beam is spatially stabilized using two controlled mirrors and two segmented photodiodes, see text for details. After spectral broadening by SPM in the neon gas, the laser pulses pass a $\lambda/4$-plate ensuring linear polarization. Chirped mirrors temporally compress the pulses and also precompensate for the dispersion on the path to the REMI. Fine-adjustment of the overall dispersion and pulse-duration is performed by movable glass-wedges

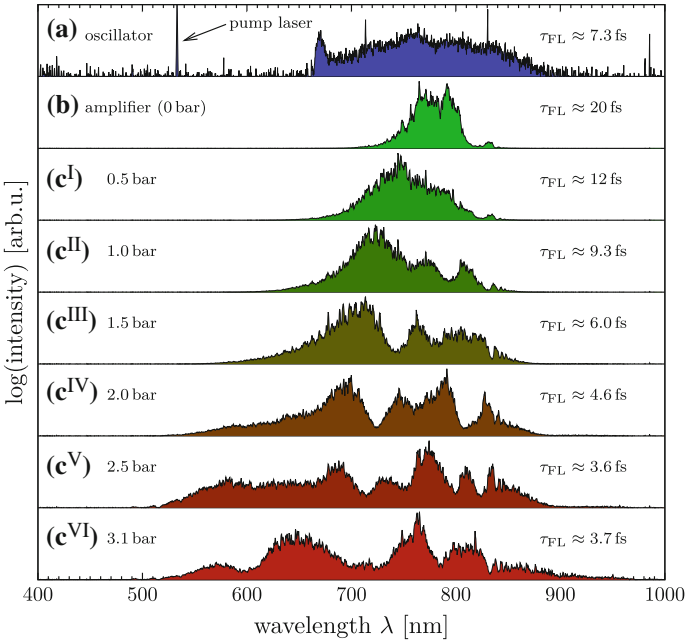

Fig. 2.4 Typical laser spectra obtained at different steps of the ultrashort pulse generation and their Fourier limits. **a** In the oscillator. **b** After the chirped mirrors and the Mach–Zehnder interferometer with an empty fiber. Apart from (*small*) losses on the optical elements this spectrum resembles the output spectrum of the femtosecond laser system. (c^{I-VIII}) Same as (**b**) but with nonzero, different absolute neon pressures in the fiber. SPM broadens the spectrum and thus reduces the Fourier limit of the pulses. In the region of short wavelengths the spectrum is suppressed by the low reflectivity of the chirped mirrors used

focus created is very elongated (see Sect. 2.1.3) and—since additionally confined in the hollow center of the fiber—extends to the full fiber length of about 1 m. Over this distance, the light can interact with neon atoms inside the hollow core, which represent the nonlinear medium for the SPM process. Since the optimal and stable incoupling into the fiber is crucial, small spatial drifts of the laser beam over time have to be efficiently compensated. For this purpose, a focus stabilization system was built [24]. It contains two four-fold segmented photodiodes where small parts of the beam are focussed on and thus small drifts can be detected. A computer can react by small adjustments with two motorized mirrors. A $\lambda/4$-plate after the fiber is used to ensure linear polarization of the light.

Chirped Mirror Compression

Due to the extremely broad spectrum, the laser pulses are very sensitive to dispersion. While traveling through optical elements and the air on the way to the spectrometer, see Chap. 4, the different frequencies in the pulses gather an individual phase, see Sect. 2.1.2. In order to compensate for this, *chirped mirrors* with an effective negative dispersion are used [41]. These mirrors are specially designed and coated such that the red components of the beam can penetrate deeper into the material and thus travel a longer distance compared to the blue. Three matched pairs of chirped mirrors are used in the experiment while each mirror is hit twice by the laser beam resulting in twelve reflexions in total. Fine tuning of the overall dispersion is performed with an additional small amount of glass, a pair of movable wedges.

Figure. 2.4b and c^{I-VIII} show spectra obtained after the chirped mirrors for different pressures of neon in the fiber. Apart from (small) losses on the optical elements, (b) resembles the output spectrum of the femtosecond laser system described in Sect. 2.2.1. However, short wavelengths around 500 nm and below are suppressed due to insufficient reflectivity of the chirped mirrors in this range. An approximation for the Fourier limit of the pulses is given for each of the spectra in Fig. 2.4, as it can be obtained by a calculation of the temporal shape of the electric field according to Eq. (2.4)[5] and a subsequent Gaussian fit to the temporal intensity distribution associated.

The duration of the pulses delivered by the system was measured to be around 6 fs before, see [16, 23], using autocorrelation and ZAP-SPIDER[6] techniques [1]. However, in order to obtain information about the pulse duration during the alignment of the setup for few-cycle pulses, in this work a *single-shot Stereo-ATI* [7] *phasemeter* [42] was utilized. Detailed information about the setup can be found in [17]. Since the quality of the CEP-signal delivered by this device depends crucially on the pulse duration [34], it can be used as a qualitative indicator for the pulse duration at least for alignment purposes, where no accurate value has to be extracted.

[5] The integral in the expression is replaced by a sum over the binned spectrum.

[6] Zero-additional-phase spectral phase interferometry for direct electric field reconstruction.

[7] Above-threshold ionization.

2.2.3 Setup for Pump-Probe Measurements

For the time-resolved *pump-probe measurements* presented in Chap. 5, two pulses are required with an adjustable time delay with respect to each other. In such experiments, the first "pump" pulse is used to start dynamics in the target system while the second pulse "probes" the state of the system after a defined and adjustable time period, during which the system is allowed to evolve freely, see e.g. [28, 38]. For the creation of the pulse-pair and the adjustment of the time-delay, a *Mach–Zehnder interferometer* is used. Detailed information about the setup can be found in [13]. Starting from a single laser pulse, a thin beam splitter is used to create two identical pulses. Each pulse travels along one of the two arms of the interferometer, see Fig. 2.5. One of the arms is equipped with a piezo-driven stage to move two mirrors and to adjust the distance s the specific pulse has to travel before the two beams are recombined by a second beam splitter. The time delay between the pulses can be controlled with high precision and a spatial shift of the stage by Δs leads to a shift in time of

$$\Delta t = 2\frac{\Delta s}{c}, \tag{2.27}$$

where c is the speed of light in air. The setup works for both ultrashort pulses from the fiber and the pulses delivered directly from the femtosecond laser system.

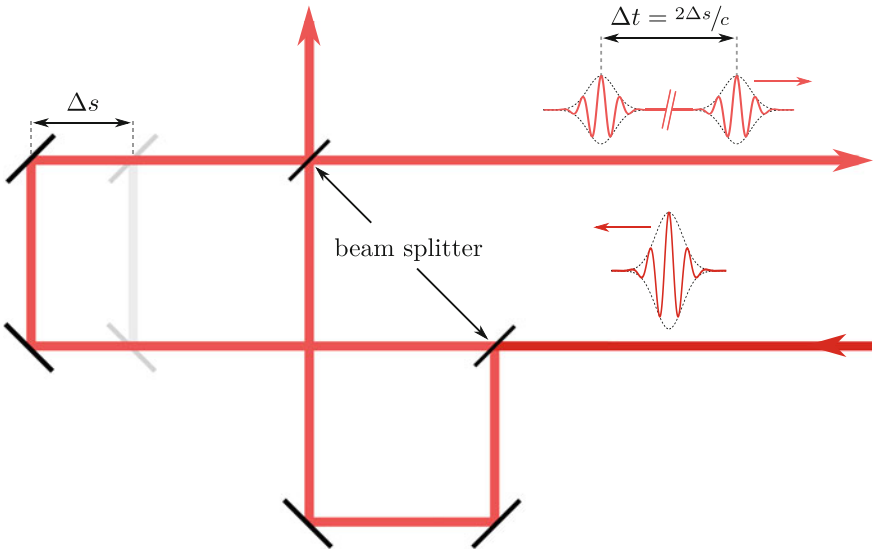

Fig. 2.5 Schematic picture of the Mach–Zehnder interferometer. The incoming pulses are split into two identical copies. The time delay of one pulse with respect to the other can be controlled by adjusting the length of one arm of the spectrometer

2.2.4 Frequency Doubling and Mixing

Nonlinear effects in suitable materials can be used to generate coherent and intense pulses at wavelengths not accessible directly for the laser system. Exposed to the strong fields of a (linearly polarized) intense laser, the electron clouds of the atoms in a nonlinear medium—e.g. a crystal made from β-barium borate (BBO)—are collectively driven back and forth. If the strength of the laser field is in the same order as the intrinsic atomic electric fields, large amplitudes are achieved in the driven oscillation. In contrast to very small amplitudes, where the oscillation has approximately harmonic character, higher orders of the effective potentials become significant. For a lossless and dispersionless medium, the polarization is given by [4, Sect. 1.1]

$$\begin{aligned} P(t) &= \chi^{(1)} E(t) + \chi^{(2)} E^2(t) + \chi^{(3)} E^3(t) + \cdots \\ &= P^{(1)}(t) + P^{(2)}(t) + P^{(3)}(t) + \cdots, \end{aligned} \tag{2.28}$$

where $\chi^{(1)}$ is the linear and $\chi^{(2)}$ and $\chi^{(3)}$ the second- and third-order nonlinear susceptibilities.[8] This relation can be utilized in different experimental schemes to generate new frequency components, initially not present in the laser spectrum. For simplicity the following discussion is restricted to monochromatic fields but can in principle be extended to the broader spectrum of short laser pulses: The phase matching conditions mentioned are then only fulfilled perfectly for the carrier frequency ω_0. However, for frequencies sufficiently close to ω_0, the processes may take place, although with reduced efficiency [4, Sects. 2.2 and 2.7]. Thus, few-cycle pulses with their very broad spectra are not suitable and in the experiments exclusively the direct output of the femtosecond laser system is utilized.

Second Harmonic Generation (SHG)

In the simplest scheme possible, the laser pulses delivered by the laser are directly focussed into the nonlinear crystal. If the electric field is described as $E(t) = E\exp(-i\omega_0 t) + \text{c.c.}$,[9] Eq. (2.28) yields [4, Sect. 1.2]

$$P^{(2)}(t) = 2\chi^{(2)} E E^* + \left[\chi^{(2)} E^2 \mathrm{e}^{-2i\omega_0 t} + \text{c.c.}\right]. \tag{2.29}$$

The spectrum of the time-dependent polarization comprises components with a frequency of $2\omega_0$ and so does the light emitted. For this reason the process is known as *second harmonic generation* (SHG). As depicted in Fig. 2.6, this can be understood as a transformation of two photons of the incident beam into one photon of the doubled frequency. In addition to the conservation of energy, a special form of momentum conservation has to be considered: For an efficient generation of second harmonic

[8] Since E and P are treated as scalar quantities, the tensor-nature of the susceptibilities $\chi^{(i)}$ is omitted [4, Sect 1.1].

[9] This description of the total electric field as a sum of a complex field and its complex conjugated expression, $E(t) = \varepsilon(t) + \text{c.c.}$, is mathematically equivalent to the description $E(t) = \text{Re}\{\varepsilon(t)\}$ used in Sect. 2.1.

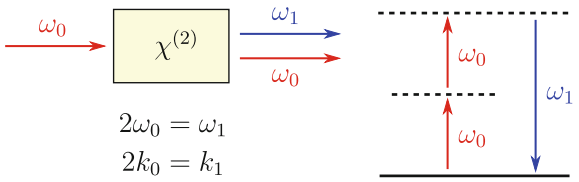

Fig. 2.6 Scheme for SHG in a nonlinear crystal. Two photons of the incident laser beam are converted into one photon of twice the frequency and energy ω_1. In the energy diagram on the right the *solid line* represents the ground state while virtual states, only existent in the presence of the laser field, are displayed as *dashed lines*. In addition, the phase matching condition, Eq. (2.30), is displayed. Scheme according to [4, Fig. 1.2.1]

radiation it is necessary that the *wavevector mismatch* vanishes [4, Sects. 2.2 and 2.6]:

$$\Delta k = 2k_0 + k_1 = 2\frac{n_0\omega_0}{c} + \frac{n_1\omega_1}{c} = 0, \tag{2.30}$$

where $\omega_1 = 2\omega_0$ and n_i is the refractive index of the nonlinear material for the respective frequency. This situation is commonly referred to as *phase matching* and Eq. (2.30) is the associated *phase matching condition*.

In particular for nonlinear crystals, birefringent properties of the material may be utilized for this purpose: By aligning the optical axis of the crystal with respect to the propagation direction of the light, n_i can be adjusted [4, Sect. 2.7].

In the experiment, a BBO crystal is used to generate second harmonic radiation from the fundamental 790 nm pulses delivered by the femtosecond laser system. Thus, pulses with a carrier wavelength of 395 nm close at the high-frequency edge of the visible and the beginning of the ultraviolet spectrum are generated. On one hand, the SHG process can only be efficient for a relatively narrow spectral region around the central carrier frequency, which suggests a longer duration for the pulses compared with those in the incoming beam. On the other hand, SHG is a nonlinear process and hence depends strongly on the laser intensity. Therefore the leading and trailing edges of the pulse can be expected to be suppressed and the pulse shortened.

Frequency Mixing: Generation of Sum and Difference (SFG and DFG)

In a modified scheme, laser pulses of two different frequencies, ω_1 and ω_2 ($\omega_1 > \omega_2$) can be focussed simultaneously into the nonlinear crystal. For the moment, the availability of pulses with two different carrier frequencies is simply postulated and will be elucidated later in Sect. 2.2.5. In analogy to the treatment of SHG, the incident beam can be described by $E(t) = E_1 \exp(-i\omega_1 t) + E_2 \exp(-i\omega_2 t) + \text{c.c.}$ and Eq. (2.28) yields [4, Sect. 1.2]

$$\begin{aligned} P^{(2)}(t) = {} & 2\chi^{(2)}\left(E_1E_1^* + E_2E_2^*\right) + \left[\chi^{(2)}\left(E_1^2\mathrm{e}^{-2\omega_1 t} + E_2^2\mathrm{e}^{-2\omega_2 t}\right) + \text{c.c.}\right] \\ & + \left[2\chi^{(2)}\left(E_1E_2\mathrm{e}^{-2(\omega_1+\omega_2)t} + E_1E_2^*\mathrm{e}^{-2(\omega_1-\omega_2)t}\right) + \text{c.c.}\right]. \end{aligned} \tag{2.31}$$

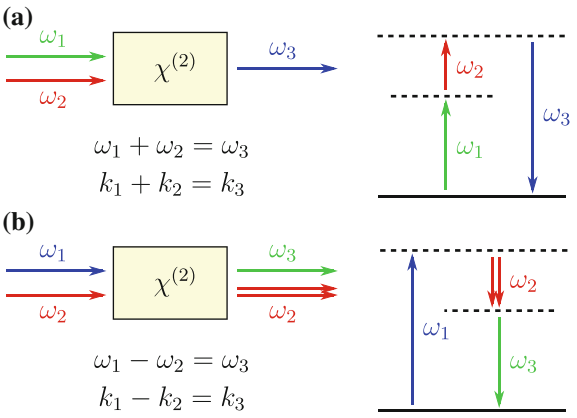

Fig. 2.7 Frequency mixing with **a** SFG and **b** DFG in a nonlinear crystal with according phase matching conditions, Eq. (2.32). DFG contains a stimulated process where the irradiated radiation of lower frequency ω_2 is coherently amplified. Schemes according to [4, Fig. 1.2.2] for (**a**) and [4, Fig. 1.2.3] for (**b**), respectively

The first two terms reflect SHG processes simultaneously but independently taking place for the two different frequencies, while the last term is arising from an interplay between them. It introduces components in the oscillations of the time-dependent polarization with both the sum $\omega_3 = \omega_1 + \omega_2$ and the difference $\omega_3 = \omega_1 - \omega_2$ of the two frequencies initially present. Thus, radiation with theses frequencies may be emitted, provided that the respective phase matching condition is met [4, Sects. 2.4 and 2.5]

$$k_1 \pm k_2 = k_3 \quad \text{for} \quad \omega_3 = \omega_1 \pm \omega_2 \tag{2.32}$$

The processes are referred to as *sum frequency generation* (SFG) and *difference frequency generation* (DFG), respectively, and depicted in Fig. 2.7. The latter is remarkable in one important aspect: DFG contains a stimulated process where the radiation of the incident lower frequency ω_2 is coherently amplified. This unique feature of DFG offers an efficient way for the creation of arbitrary frequencies, technically utilized as described in the following section.

2.2.5 *Wavelength Tuning Using an OPA System*

For creation of pulses with arbitrary carrier frequencies directly from the pulses delivered by the femtosecond laser system, several nonlinear effects may be combined, namely SPM followed by DFG and optional subsequent SHG, SFG or DFG. The experimental scheme presented in the following is refereed to as *optical parametric amplifier* (OPA). Here, only a brief description of the working principle is given, composed from [7] and [4, Sect. 2.8].

As discussed in Sect. 2.2.2, SPM in non-linear materials can be used for the generation of frequency components initially not present in the laser beam. Thus, a continuum of white light can be produced by focusing a part of the laser beam into

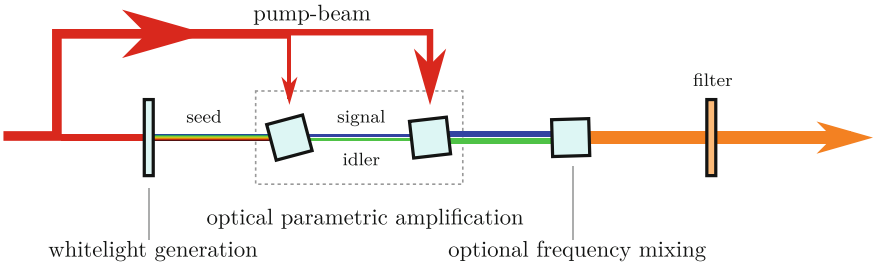

Fig. 2.8 Working principle of the OPA system: The pump beam is delivered by the femtosecond laser system. A small part of the beam creates a continuum of *white* light due to SPM in a sapphire plate. Any frequency generated can serve as seed for an DFG process in a nonlinear crystal. Here, the energy of one pump photon is used for the amplification of the seed beam and additional generation of an idler photon. The signal beam is further amplified in a second OPA stage, again producing an additional strong idler beam. Subsequent frequency doubling (SHG) or mixing (SFG, DFG) of residual pump, signal and idler beam is optionally possible. A filter finally removes the undesired frequencies before the pulses are guided to the experiment

e.g. a sapphire plate. A desired wavelength of this continuum may be used together with radiation of the initial wavelength of 790 nm for a DFG process in a nonlinear crystal. Since energy conservation has to be fulfilled, the chosen wavelength has to be larger than 790 nm. In this context it is convenient to refer to the different beams coupled into the crystal as *seed* and *pump* beam, respectively, see Fig. 2.8. A part of the energy of one photon from the pump beam is used for amplification of the seed beam by stimulated emission. In addition, a second photon of a different wavelength is formed using the remaining energy. The process may also be carried out in a two-step amplification scheme involving two nonlinear crystals, representing a pre- and a power amplifier. Hence, a *signal* and *idler* beam are generated where one is the amplified seed. In the following—as commonly defined—the signal represents the beam with the higher photon energy.

By rotation of the nonlinear crystal and thereby achieving phase matching for a particular combination of signal and idler wavelengths, the carrier frequency of the generated pulses can be controlled over a large range. After the OPA, pulses with three different carrier frequencies are usually available: The remaining part of the pump beam delivered by the laser as well as the signal and the idler beam. Subsequent frequency doubling or mixing by SHG, SFG or DFG may be used and extends the region of accessible wavelengths.

In the experiment a commercial *Light Conversion* "TOPAS-C" OPA system is used containing two OPA amplification stages and subsequent optional frequency doubling (SHG) or mixing (SFG, DFG) [26]. Downstream filters containing highly reflective mirrors for the desired wavelength ensure sufficient suppression of other radiation. The polarization of the emitted radiation depends on the generation mechanism and is either horizontal or vertical after the OPA. Two different periscopes are used to guide the beam to the REMI such that the polarization is finally aligned along the spectrometer axis in either case as shown in Fig. 4.1.

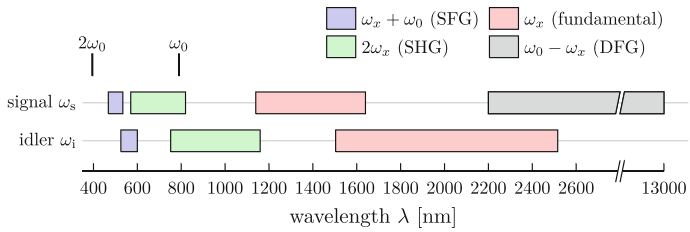

Fig. 2.9 Wavelengths accessible with the OPA system for pump wavelength of $\omega_0 = 790\,\text{nm}$. Different production schemes deliver wavelengths over the full visible to infrared spectrum (ranges according to "WinTOPAS 3.0.12" control software delivered with the system). In addition, the harmonic frequency $2\omega_0$ is shown accessible by SHG of ω_0

Figure 2.9 gives an overview about the different production mechanisms made available by the OPA and the accessible wavelengths. It is noteworthy that—in principle—the full range from around 470 nm to around 13000 nm can be accessed. However, due to strongly deviating efficiencies of the different processes, strong-field experiments are restricted to a region below approximately 1600 nm. Before entering the OPA, the spectrum of the femtosecond laser system is slightly narrowed to a width of about 30 nm around the central wavelength in order to facilitate the overall phase matching. The signal and idler pulses are expected to have a duration of $0.7 - 1$ times the duration of the pump pulses [27]. Thus, the pulse duration can be roughly estimated to be at least about 20 fs or longer.

References

1. P. Baum et al., Zero-additional-phase SPIDER: full characterization of visible and sub-20-fs ultraviolet pulses. Opt. Lett. **29**, 210–212 (2004). doi:10.1364/OL.29.000210
2. G.D. Boyd, J.P. Gordon, Confocal multimode resonator for millimeter through optical-wavelength masers. Bell Syst. Tech. J. **40**, 489–508 (1961). doi:10.1002/j.1538-7305.1961.tb01626.x
3. G.D. Boyd, H. Kogelnik, Generalized confocal resonator theory. Bell Syst. Tech. J. **41**, 1347–1369 (1962). doi:10.1002/j.1538-7305.1962.tb03281.x
4. R.W. Boyd, *Nonlinear Optics* (Academic Press, Boston, 2003)
5. T. Brabec, F. Krausz, Intense few-cycle laser fields: frontiers of nonlinear optics. Rev. Mod. Phys. **72**, 545–591 (2000). doi:10.1103/RevModPhys.72.545
6. I.N. Bronstein et al., *Taschenbuch der Mathematik* (Europa-Lehrmittel, 2005)
7. G. Cerullo, S. De Silvestri, Ultrafast optical parametric amplifiers. Review of Scientific Instruments **74**, 1–18 (2003). doi:10.1063/1.1523642
8. W. Demtröder, *Laser Spectroscopy* (Springer, Berlin, 2003)
9. W. Demtröder, *Experimentalphysik 2: Elektriziät und Optik* (Springer-Verlag, Berlin Heidelberg New York, 2004)
10. J.C. Diels, W. Rudolph, *Ultrashort Laser Pulse Phenomena* (Academic Press, Boston, 2006)
11. J. Eichler, H.J. Eichler, *Laser—Bauformen, Strahlführung, Anwendungen* (Springer, New York, 2010)
12. R. Ell et al., Generation of 5-fs pulses and octave-spanning spectra directly from a Ti:sapphire laser. Opt. Lett. **26**, 373–375 (2001). doi:10.1364/OL.26.000373

13. T. Ergler, Zeitaufgelöste Untersuchungen zur Fragmentationsdynamik von H_2 (D_2) in ultrakurzen Laserpulsen. Ph.D. thesis. Ruperto-Carola University of Heidelberg, Germany. URN: urn:nbn:de:bsz:16-heidok-67240 (2006)
14. User's manual for Mirror-dispersion-controlled Ti:Sapphire Oscillator FEMTOSOURCE Rainbow seed. FEMTOLASERS Produktions GmbH (2006)
15. FEMTOPOWER compact pro CE-PHASE HP/HR Femtosecond Multi-pass Amplifier USER'S MANUAL v. 3.2. FEMTOLASERS Produktions GmbH
16. B. Fischer, Time resolved studies of H_2^+ dissociation with phase-stabilized laser pulses. Ph.D. thesis. Ruperto-Carola University of Heidelberg, Germany. URN: urn:nbn:de:bsz:16-heidok-107569 (2010)
17. C. Hofrichter, A stereo electron spectrometer for carrier-envelope phase measurements of fewcycle laser pulses, MA thesis. Ruperto-Carola University of Heidelberg, Germany (2009)
18. U. Keller, Ultrafast solid-state laser oscillators: a success story for the last 20 years with no end in sight. Appl. Phys. B: Lasers Opt. **100**, 15–28 (2010). doi:10.1007/s00340-010-4045-3
19. U. Keller et al., Femtosecond pulses from a continuously self-starting passively mode-locked Ti:sapphire laser. Opt. Lett. **16**, 1022–1024 (1991). doi:10.1364/OL.16.001022
20. Ursula Keller et al., Semiconductor saturable absorber mirrors (SESAM's) for femtosecond to nanosecond pulse generation in solid-state lasers. IEEE J. Sel. Top. Quantum Electron. **2**, 435–453 (1996). doi:10.1109/2944.571743
21. Fritz Kurt Kneubühl and Markus Werner Sigrist. Laser. Vierweg + Teubner (2008)
22. F. Krausz et al. (ed.), *Ultrafast Optics IV* (Springer, LLC, New York, 2004)
23. M. Kremer, Einfluß der Träger-Einhüllenden-Phase auf die Wechselwirkung ultrakurzer Laserpulse mit Molekülen, Ph.D. thesis. Ruperto-Carola University of Heidelberg, Germany. URN: urn:nbn:de:bsz:16-heidok-100544 (2009)
24. A. Krupp, Untersuchung der Pulsdauer und Langzeitstabilisierung eines Hohlfaserkompressors, BA thesis. Ruperto-Carola University of Heidelberg, Germany (2011)
25. M. Lenzner et al., Sub-20-fs, kilohertz-repetition-rate Ti:sapphire amplifier. Opt. Lett. **20**, 1397–1399 (1995). doi:10.1364/OL.20.001397
26. TOPAS-C, Traveling-wave Optical Parametric Amplifier of Superfluorescence, User's Manual. Light Conversion Ltd. (2006)
27. TOPAS-C specification sheet. http://www.lightcon.com/upload/iblock/a86/a86f4da6ccbf3c724a18148a8cc852a3.pdf, Accessed 22 July 2014. Light Conversion Ltd. (2014)
28. A. Mokhtari et al., Direct femtosecond mapping of trajectories in a chemical reaction. Nature **348**, 225–227 (1990). doi:10.1038/348225a0
29. G.G. Paulus et al., Absolute-phase phenomena in photoionization with few-cycle laser pulses. Nature **414**, 182–184 (2001). doi:10.1038/35102520
30. J.H. Posthumus, The dynamics of small molecules in intense laser fields. Rep. Progr. Phys. **67**, 623–665 (2004). doi:10.1088/0034-4885/67/5/R01
31. J.H. Posthumus, J.F. McCann, Diatomic molecules in intense laser fields. In: *Molecules and Clusters in Intense Laser Fields*, ed. by J. Posthumus (Cambridge University Press, Cambridge, 2001). Chap. 2, pp. 27–77
32. T. Rathje et al., Review of attosecond resolved measurement and control via carrier-envelope phase tagging with above-threshold ionization. J. Phys. B: Atom. Mol. Opt. Phys. **45**, 074003 (2012). doi:10.1088/0953-4075/45/7/074003
33. S. Sartania et al., Generation of 0.1-TW 5-fs optical pulses at a 1-kHz repetition rate. Opt. Lett. **22**, 1562–1564 (1997). doi:10.1364/OL.22.001562
34. A.M. Sayler et al., Real-time pulse length measurement of few-cycle laser pulses using above-threshold ionization. Opt. Exp. **19**, 4464–4471 (2011). doi:10.1364/OE.19.004464
35. A.S. Siegmann, *Lasers* (University Science Books, USA, 1986)
36. Ch. Spielmann et al., Compact, high-throughput expansion-compression scheme for chirped pulse amplification in the 10 fs range. Opt. Commun. **120**, 321–324 (1995). doi:10.1016/0030-4018(95)00494-S
37. A. Stingl et al., Sub-10-fs mirror-dispersion-controlled Ti:sapphire laser. Opt. Lett. **20**, 602–604 (1995). doi:10.1364/OL.20.000602

38. Albert Stolow et al., Femtosecond time-resolved photoelectron spectroscopy. Chem. Rev. **104**, 1719–1758 (2004). doi:10.1021/cr020683w
39. Donna Strickland, Gerard Mourou, Compression of amplified chirped optical pulses. Opt. Commun. **56**, 219–221 (1985). doi:10.1016/0030-4018(85)90120-8
40. O. Svelto, in *Principles of Lasers*, ed. by David C. Hanna. (Plenum Press, New York, 1998)
41. R. Szipöcs et al., Chirped multilayer coatings for broadband dispersion control in femtosecond lasers. Opt. Lett. **19**, 201–203 (1994). doi:10.1364/OL.19.000201
42. T. Wittmann et al., Single-shot carrier-envelope phase measurement of few-cycle laser pulses. Nat. Phys. **5**, 357–362 (2009). doi:10.1038/nphys1250

http://www.springer.com/978-3-319-32045-8

High-Resolution Experiments on Strong-Field Ionization of Atoms and Molecules
Test of Tunneling Theory, the Role of Doubly Excited States, and Channel-Selective Electron Spectra

Fechner, L.

2016, XIV, 151 p. 71 illus., 29 illus. in color., Hardcover
ISBN: 978-3-319-32045-8